Bone 75 (2015) 55–61

Contents lists available at ScienceDirect

Bone

journal homepage: www.elsevier.com/locate/bone

Original article

Development of an *in vivo* rabbit ulnar loading model

Andrew P. Baumann [a], Mohammad W. Aref [b], Travis L. Turnbull [a], Alex G. Robling [b], Glen L. Niebur [a], Matthew R. Allen [b], Ryan K. Roeder [a,*]

[a] Department of Aerospace and Mechanical Engineering, University of Notre Dame, Notre Dame, IN 46556, USA
[b] Department of Anatomy and Cell Biology, Indiana University School of Medicine, Indianapolis, IN 46202, USA

ARTICLE INFO

Article history:
Received 3 October 2014
Revised 30 December 2014
Accepted 28 January 2015
Available online 12 February 2015

Edited by David Fyhrie

Keywords:
Adaptation
Cortical bone
In vivo loading
Modeling
Rabbit ulna
Remodeling

ABSTRACT

Ulnar and tibial cyclic compression in rats and mice have become the preferred animal models for investigating the effects of mechanical loading on bone modeling/remodeling. Unlike rodents, rabbits provide a larger bone volume and normally exhibit intracortical Haversian remodeling, which may be advantageous for investigating mechanobiology and pharmaceutical interventions in cortical bone. Therefore, the objective of this study was to develop and validate an *in vivo* rabbit ulnar loading model. Ulnar tissue strains during loading of intact forelimbs were characterized and calibrated to applied loads using strain gauge measurements and specimen-specific finite element models. Periosteal bone formation in response to varying strain levels was measured by dynamic histomorphometry at the location of maximum strain in the ulnar diaphysis. Ulnae loaded at 3000 microstrain did not exhibit periosteal bone formation greater than the contralateral controls. Ulnae loaded at 3500, 4000, and 4500 microstrain exhibited a dose-dependent increase in periosteal mineralizing surface (MS/BS) compared with contralateral controls during the second week of loading. Ulnae loaded at 4500 microstrain exhibited the most robust response with significantly increased MS/BS at multiple time points extending at least 2 weeks after loading was ceased. Ulnae loaded at 5250 microstrain exhibited significant woven bone formation. Rabbits required greater strain levels to produce lamellar and woven bone on periosteal surfaces compared with rats and mice, perhaps due to lower basal levels of MS/BS. In summary, bone adaptation during rabbit ulnar loading was tightly controlled and may provide a translatable model for human bone biology in preclinical investigations of metabolic bone disease and pharmacological treatments.

Introduction

Animal models for *in vivo* skeletal loading have been essential in advancing understanding of the relationships between mechanical loading and bone modeling/remodeling [1]. Early models enabling extrinsic control of load levels provided significant knowledge but typically employed invasive surgical procedures, such as pinning and external fixation [1–4], which can present complications (e.g., infection and inflammation) in experiments and interpretation of results. Therefore, non-invasive extrinsic loading models were developed, including four-point bending [5] and cantilever bending [6] of rodent tibiae, axial impact loading of rabbit tibiae [7], and cyclic compression of rodent ulnae [8–16] and tibiae [17–19].

Over the past decade, ulnar and tibial cyclic compression have become preferred models due to utilization of non-invasive extrinsic loading without soft tissue inflammation, applicability to both rats and mice, and reproducibility for studying periosteal bone formation [9–13,16,17]. These models have elucidated the effects of loading magnitude [9–11,16,17], frequency [9,11], and duration [12] on adaptation via periosteal bone formation. However, limitations of these models include a relatively small bone volume for preparing post-mortem tissue test specimens, limited cortical bone loss in response to estrogen depletion, and the absence of normal intracortical Haversian remodeling in rodents [1,20–23].

In this study, we propose a rabbit ulnar loading model patterned after the established rodent ulnar loading model. The rabbit ulna exhibits natural curvature such that axial compression of the forelimb transfers load to the ulna from the flexed carpus and olecranon process, inducing a bending moment (Fig. 1), similar to rodents [1,14]. In contrast to rodents, adult rabbits naturally undergo intracortical Haversian remodeling [22–27], providing a more translatable model to humans for studying cortical bone. Moreover, rabbits are known to respond to parathyroid hormone (PTH) [25,26], bisphosphonates [28,29], cathepsin K inhibitors [29], and ovariectomy [29]. As such, rabbits could provide an alternative model for preclinical pharmaceutical investigations, which may otherwise require nonhuman primates [29].

Therefore, the objective of this study was to develop and validate a rabbit ulnar loading model (Fig. 1) suitable for investigations of cortical bone mechanobiology. Periosteal bone formation in rabbit ulnae was

* Corresponding author at: Department of Aerospace and Mechanical Engineering, Bioengineering Graduate Program, 148 Multidisciplinary Research Building, University of Notre Dame, Notre Dame, IN 46556, USA.
E-mail address: rroeder@nd.edu (R.K. Roeder).

http://dx.doi.org/10.1016/j.bone.2015.01.022
8756-3282/

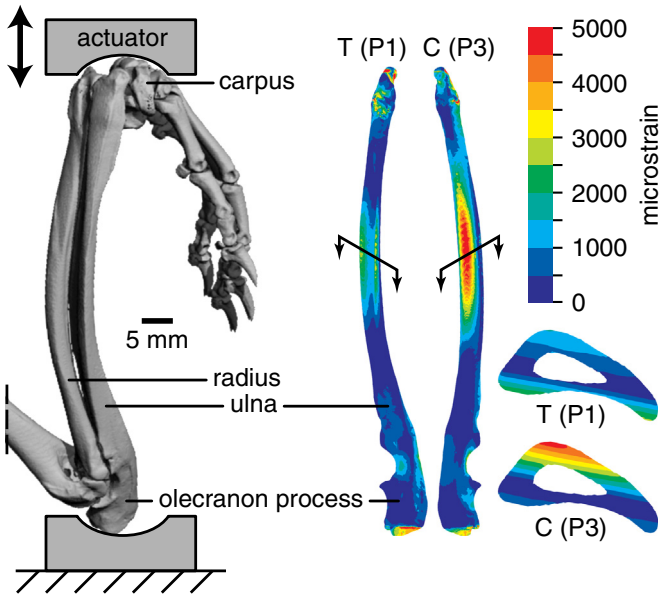

Fig. 1. Segmented, 3-D micro-CT reconstruction of the right rabbit forelimb positioned within a schematic loading fixture. Compressive uniaxial loading of the forelimb transferred load from the flexed carpus and olecranon process to the ulna, inducing a cranial–caudal bending moment due to the curvature of the ulna. Specimen-specific finite element model predictions of the principal strain distribution for an applied static uniaxial compressive load (e.g., 100 N shown) showed that maximum tensile (T, P1) and compressive (C, P3) principal strains were located on cranial and caudal periosteal surfaces, respectively, within the distal mid-diaphysis of the ulna. Note that model predictions were calibrated by measured strains during static uniaxial compression.

hypothesized to exhibit a dose-dependent anabolic response to ulnar loading. Ulnar tissue strains during loading of intact forelimbs were characterized and calibrated to applied loads using strain gauge measurements and specimen-specific finite element models. Periosteal bone formation in response to varying strain levels was measured by dynamic histomorphometry at the location of maximum strain in the ulnar diaphysis using a quadruple fluorochrome labeling technique.

Materials and methods

Animals

Female New Zealand white rabbits (Covance Research Products, Denver, PA) were obtained as retired breeders at 8–12 (10.4 ± 1.1) months of age, such that all animals were beyond skeletal maturity [30]. As-received rabbits for all experiments ($N = 27$) exhibited a mean (±standard deviation) body mass of 3.9 (0.3) kg. Of these, 8 rabbits were used for characterizing load-strain calibrations, 4 rabbits were used for an *in vivo* ulnar loading pilot study to identify the strain levels required to induce periosteal bone formation, and 15 rabbits were used for a final *in vivo* ulnar loading study to measure periosteal bone formation by dynamic histomorphometry. Rabbits were housed in individual cages, allowed unrestricted movement and *ad libitum* access to food and water at all times, and were given 3 days to acclimate prior to initiating experiments. At the conclusion of each experiment, rabbits were euthanized by intravenous overdose of sodium pentobarbital (0.2 ml/kg, Somnasol, Butler-Schein, Dublin, OH), followed by bilateral pneumothorax. All experimental procedures were approved by the Institutional Animal Care and Use Committee at the University of Notre Dame prior to the initiation of the study.

Static and dynamic load-strain calibrations

Specimen-specific finite element models were used to identify locations of maximum periosteal strains during ulnar loading (Fig. 1). Eight rabbits (10.8 ± 0.7 months of age, 4.2 ± 0.2 kg) were received and immediately sacrificed. Right and left forelimbs were removed and imaged intact via micro-CT (μCT-80, Scanco Medical AG, Brüttisellen, Switzerland) at 70 kVp, 114 μA, 400 ms integration time, and 74 μm resolution for 250 projections per slice with image slices oriented perpendicular to the ulnar diaphysis. Bone was segmented from soft tissue at threshold values which corresponded to a tissue mineral density of ~530 mg hydroxyapatite per cubic centimeter (mg HA/cm^3) using a custom calibration phantom [31]. Segmented bone images were converted to finite element meshes of constant strain four-node tetrahedrons using a marching cubes algorithm (Visualization Toolkit, Kitware, Clifton Park, NY) [32]. The first principal strain and von Mises stress at the location of maximum periosteal strain converged to less than 5% difference at 100 μm when the element size was varied between 140 and 90 μm in 10 μm increments. Finite element analyses (ADINA v8.8, ADINA R&D, Inc., Watertown, MA) simulated uniaxial compression with a distributed static load applied to the proximal epiphyses and boundary conditions that mimicked the loading fixtures described below. Surface nodes at the distal epiphyses were constrained for both lateral and longitudinal translation; surface nodes at the proximal epiphyses were constrained for lateral translation. Material properties in fully elastic analyses initially utilized an isotropic elastic modulus of 25 GPa [33] and Poisson's ratio of 0.3 to guide the placement of strain gauges on periosteal surfaces.

A static load-strain calibration was determined by mounting single-element strain gauges (Vishay Measurements Group, Inc., Raleigh, NC) to left ulnae ($n = 8$) within intact forelimbs through small incisions at locations of maximum tensile and compressive principal strains on periosteal surfaces, as determined by the initial finite element models. One ulna was removed from the study due to debonding of the strain gauge during loading. Forelimbs were loaded (ElectroForce 3300, Bose Corp., Eden Prairie, MN) to failure in static uniaxial compression at a displacement rate of 1 mm/s to minimize strain rate effects. Custom stainless steel loading fixtures with a hemispherical cup (25 mm radius) were used to cradle the flexed carpus and olecranon process of the forelimb during loading (Fig. 1). Axial load-strain data for each forelimb was fit using linear least squares regression to generate a static load-strain calibration from the pooled data. Finite element models were subsequently calibrated by the measured axial strains in order to account for material properties and load sharing between the radius and ulna. Periosteal strains in the models were determined by three-node triangular shell elements of negligible modulus placed at strain gage locations. A mean homogenous tissue modulus was obtained by minimizing error between the shell element strains and the measured strains across all ulnae. The axial strain distribution on periosteal surfaces along the length and around the perimeter of the ulnar diaphysis was plotted as the mean (±standard deviation) from the pooled specimen-specific finite element models.

A dynamic load-strain calibration was also determined by mounting strain gauges (Vishay) to right ulnae ($n = 8$) within intact forelimbs through small incisions at locations of maximum tensile and compressive axial strains on periosteal surfaces, as determined by the calibrated finite element models. Forelimbs were loaded (ElectroForce 3220, Bose Corp., Eden Prairie, MN) in cyclic uniaxial compression at 2 Hz for a total of 360 cycles at sequentially increasing peak loads of 8 to 144 N, in 8 N increments for 20 cycles per load level, and the mean peak strain amplitude was measured at each load level [10,15]. Axial load-strain data for each forelimb were fit using linear least squares regression to generate a dynamic load-strain calibration from the pooled data.

In vivo ulnar loading

Periosteal bone formation in response to *in vivo* ulnar loading was measured in response to peak compressive strain levels ranging from 3000 to 5250 microstrain. In an initial pilot study, both forelimbs of 4 rabbits (10.9 ± 0.6 months of age, 3.5 ± 0.2 kg) were loaded at peak

ulnar compressive strain levels of 3000, 3750, 4500, and 5250 microstrain ($n = 2$ forelimbs per strain level, randomly distributed among rabbits) to determine strain thresholds for inducing lamellar and woven bone formation. Subsequently, 15 rabbits (10.0 ± 1.3 months of age, 3.8 ± 0.2 kg) were randomly divided into three groups ($n = 5$/group) loaded at peak ulnar compressive strains of 3500, 4000, and 4500 microstrain in right forelimbs while left forelimbs served as contralateral controls. In both experiments, rabbits were allowed to acclimate for 3 days and received daily ulnar loading for 5 consecutive days on days 3–7 and 10–14 [9,10] (Fig. 2). Forelimbs were loaded in cyclic uniaxial compression for 360 cycles/day at 2 Hz [9] (Bose ElectroForce 3220). Peak load levels for the desired peak ulnar compressive strains were determined from the dynamic load-strain calibration. Rabbits were anesthetized during ulnar loading using an intramuscular injection of ketamine (25 mg/kg at 100 mg/ml, Butler-Schein), xylazine (5 mg/kg at 20 mg/ml, Lloyd Laboratories, Shenandoah, IA), and acepromazine (2.5 mg/kg at 10 mg/ml, Phoenix Pharmaceuticals Inc., St. Joseph, MO), supplemented with inhaled isoflurane as-needed. Recovery from anesthesia was assisted with heating pads and intravenous injection of yohimbine (0.4 mg/rabbit at 2 mg/ml, Lloyd Laboratories) as an antagonist for xylazine and ketamine [34]. There were no signs of pain or distress during or following ulnar loading.

Histomorphometry

Periosteal bone formation was measured by histomorphometry after quadruple labeling [27] with tetracycline (30 mg/kg at 30 mg/ml oxytetracycline hydrochloride, Sigma-Aldrich, St. Louis, MO), alizarin (25 mg/kg at 30 mg/ml alizarin-3-methyliminodiacetic acid, Sigma), calcein (10 mg/kg at 20 mg/ml calcein, Sigma), and xylenol orange (90 mg/kg at 90 mg/ml xylenol orange tetrasodium salt, Sigma). Each label was administered on two consecutive days beginning on day 7, 14, 21, and 28 for the four labels, respectively (Fig. 2). The daily dose of each fluorochrome label was divided in half and administered by intramuscular injection in each hind limb, such that the delivered volume was ~2 ml/site [35].

After rabbits were sacrificed on day 35 (Fig. 2), ulnae were collected, fixed in 10% neutral buffered formalin, stored in 70% ethanol, and embedded in polymethylmethacrylate. Histologic sections (~100 μm in thickness) were cut from a 10 mm segment of the ulnar diaphysis centered at the location of maximum axial compressive and tensile strain using a diamond wire saw. Sections were mounted on glass slides, ground to a final thickness of ~50 μm, and analyzed using a standard microscope with an epifluorescence lightsource and digital measurement software (BIOQUANT®, Nashville, TN).

Primary histomorphometric data were collected on the periosteal and endosteal bone surfaces. For each sequential fluorochrome label pair, measures included the length of the total bone perimeter (B.Pm), single label perimeter (sL.Pm), double label perimeter (dL.Pm), and the interlabel distance (IrL.D). From these, mineralizing surface (MS/BS = [0.5 · sL.Pm + dL.Pm]/B.Pm; %), mineral apposition rate (MAR = IrL.D/7; μm/day), and bone formation rate (BFR/BS = MS/BS · MAR · 3.65; $\mu m^3/\mu m^2$/year) were calculated [36]. All measured data for dynamic histomorphometry are available in the Appendix as Supplementary Content. Outcome measures were compared between loaded and control ulnae across strain levels using a mixed-model two-way analysis of variance (ANOVA) (JMP 10.0, SAS Institute Inc., Cary, NC). *Post hoc* comparisons were performed using a Mann–Whitney *U*-test due to a non-normal distribution of MS/BS in the overall population ($p < 0.005$, Shapiro–Wilk *W*-test) and a small sample size ($n = 5$/group). Comparisons between loaded ulnae and contralateral controls at each strain level were performed using paired *t*-tests. The level of significance was set at $p < 0.05$ for all tests.

Results

Ulnar strain distribution and load-strain calibrations

Segmented micro-CT reconstructions of intact rabbit forelimbs and specimen-specific finite element models of ulnae showed that the ulna exhibits curvature such that axial compression of the forelimb transfers load to the ulna from the flexed carpus and olecranon process, inducing a cranial-caudal bending moment (Fig. 1). Specimen-specific finite element models under static loading identified the mean (±standard deviation) location of maximum tensile and compressive strains at 32.5 (1.2) and 31.6 (1.6) mm from the distal end of ulnae (Fig. 1), which corresponded to 39.7 (2.0) and 38.5 (2.1) percent of the total ulnar length of 82.0 (2.5) mm, respectively (Fig. 3a). Maximum tensile and compressive strains were also observed to be located on cranial and caudal periosteal surfaces of ulnae, respectively (Figs. 1 and 3b). Differences between the magnitude and location of maximum principal and axial strains at the mid-diaphysis were negligible for both individual animals and pooled animals, as expected.

Ulnar strain levels in the specimen-specific finite element models were calibrated by strain gauge measurements at locations of maximum tensile and compressive strains during static loading of intact forelimbs. After calibration, the mean homogenous tissue modulus in specimen-specific finite element models of ulnae was 17.3 GPa. The measured static and dynamic (cyclic) load-strain calibrations were both linear over the range of applied axial loads (Fig. 4). Compressive strains were greater than tensile strains, as expected (Fig. 4). The dynamic load-strain calibration (Fig. 4b) was subsequently used to set load levels to target the desired peak strain levels during *in vivo* ulnar loading experiments.

In vivo ulnar loading and periosteal bone formation

An initial pilot study qualitatively revealed a dose-dependent anabolic response to *in vivo* ulnar loading (Fig. 5). Both nonloaded control ulnae and ulnae loaded at 3000 microstrain did not produce measurable levels of periosteal bone formation as evidenced by minimal labeled surface and undetectable interlabel separation (not shown). Ulnae loaded at 3500 microstrain exhibited a detectable but very weak response with minimal labeled surface and minimal interlabel separation (Fig. 5a). Ulnae loaded at 4000 and 4500 microstrain produced new lamellar bone on periosteal surfaces with 4500 microstrain providing the most robust response shown by interlabel spacing (Figs. 5b and c). Ulnae loaded at 5250 microstrain exhibited significant woven bone formation (Fig. 5d).

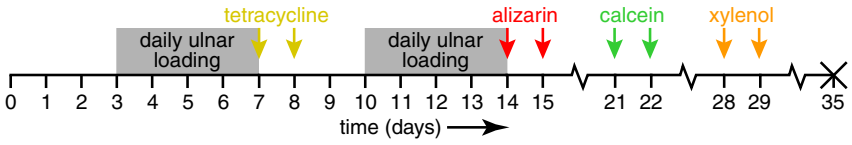

Fig. 2. The experimental design and timeline for *in vivo* ulnar loading experiments. All rabbits were allowed to acclimate for 3 days after receipt, received daily ulnar loading for five consecutive days on days 3–7 and 10–14 while under anesthesia, and were sacrificed on day 35. Periosteal bone formation was measured by histomorphometry after quadruple labeling with tetracycline, alizarin, calcein, and xylenol orange administered on two consecutive days beginning on day 7, 14, 21, and 28, respectively.

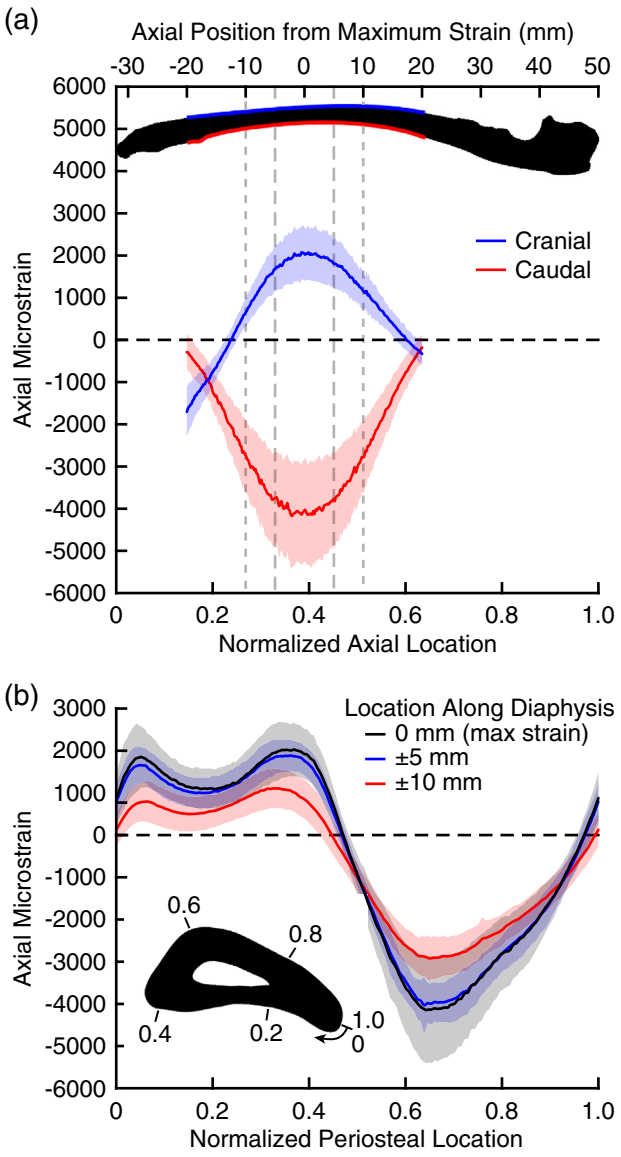

Fig. 3. The periosteal axial strain distribution (a) along the length and (b) around the perimeter of the ulnar diaphysis due to a 100 N static load showing the mean and standard deviation (shaded) from the pooled specimen-specific finite element models, which were calibrated by measured strains during static uniaxial compression. Cranial and caudal periosteal surfaces were under tension and compression, respectively, as expected due to the curvature of the ulna. Peak axial strain magnitudes occurred slightly distal of the mid-diaphysis and were reasonably consistent within ±5 mm of the maximum but were significantly diminished at ±10 mm of the maximum.

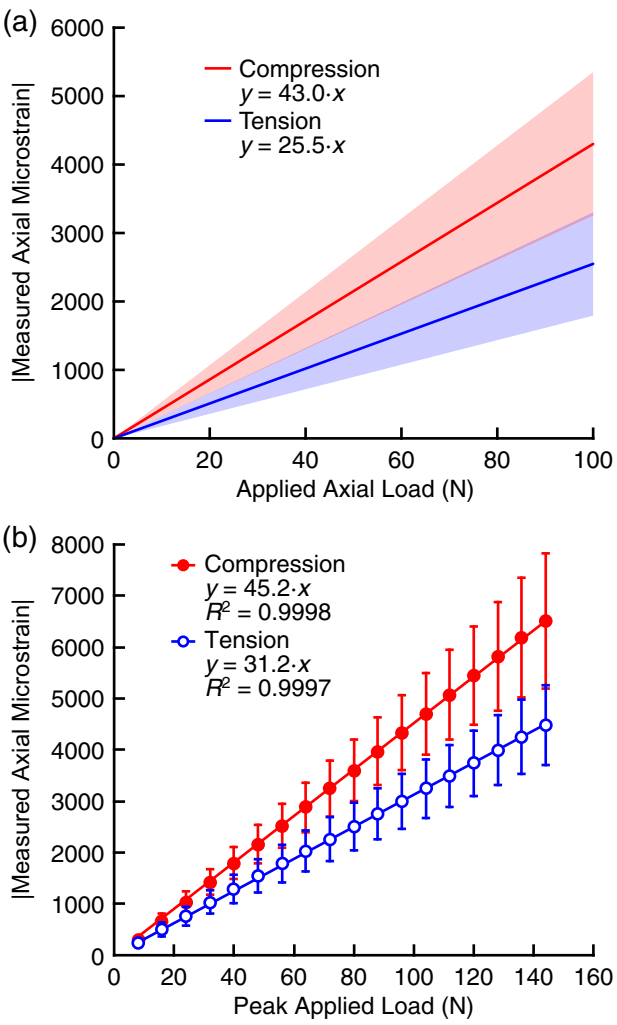

Fig. 4. Load-strain calibrations determined by strain gauge measurements at locations of maximum tensile and compressive strains during (a) static and (b) dynamic (cyclic) loading of rabbit forelimbs ($n = 8$) in uniaxial compression showing (a) the mean (line) and standard deviation (shading) of continuous data for each specimen after fitting by linear least squares regression and (b) the mean (data points) and standard deviation (error bars) of discrete data for each specimen, as well as the best fit line using linear least squares regression.

Quantitative measurements of the mineralizing surface (MS/BS) at three strain levels (3500, 4000, and 4500 microstrain) subsequently showed that lamellar periosteal bone formation exhibited a dose-dependent anabolic response to *in vivo* ulnar loading (Fig. 6). Ulnae loaded at 4500 microstrain exhibited increased MS/BS compared with contralateral controls ($p < 0.05$ loaded > control, paired *t*-test) for each label pair (Fig. 6), which characterized three time points extending at least 2 weeks after loading was ceased (Fig. 2). Ulnae loaded at 3500 and 4000 microstrain exhibited increased MS/BS compared with contralateral controls ($p < 0.05$ loaded > control, paired *t*-test) for the tetracycline-alizarin label pair (Fig. 6), which characterized the first time point concluding after the second week of loading (Fig. 2), but not at later time points after loading was ceased (Fig. 6). MS/BS exhibited an overall increase with increased strain levels for each interlabel pair ($p < 0.05$, ANOVA). Pairwise differences between strain levels within both loaded ulnae and contralateral controls were not statistically significant.

The periosteal mineral apposition rate (MAR) was able to be consistently measured for only the tetracycline-alizarin and alizarin-calcein label pairs in ulnae loaded at 4500 microstrain. The mean (±standard deviation) MAR in loaded ulnae and contralateral controls was 1.38 (0.38) and 1.23 (0.12) μm/day, respectively, for the tetracycline-alizarin label pair, and 1.46 (0.56) and 1.19 (0.12) μm/day, respectively, for the alizarin-calcein label pair. Differences in MAR between loaded ulnae and contralateral controls were not statistically significant ($p > 0.45$, paired *t*-test). The mean (±standard deviation) BFR/BS in loaded ulnae and contralateral controls was 215 (136) and 113 (86) $\mu m^3/\mu m^2$/year, respectively, for the tetracycline-alizarin label pair, and 212 (110) and 62 (25) $\mu m^3/\mu m^2$/year, respectively, for the alizarin-calcein label pair. Differences in BFR/BS between loaded ulnae and contralateral controls were statistically significant ($p < 0.05$ loaded > control, paired *t*-test).

In contrast to periosteal bone formation, endosteal bone formation did not exhibit a detectable dose-dependent response to *in vivo* ulnar loading. Tetracycline-alizarin and calcein-xylenol orange labels were too minimal for reliable measurement. Endosteal MS/BS for

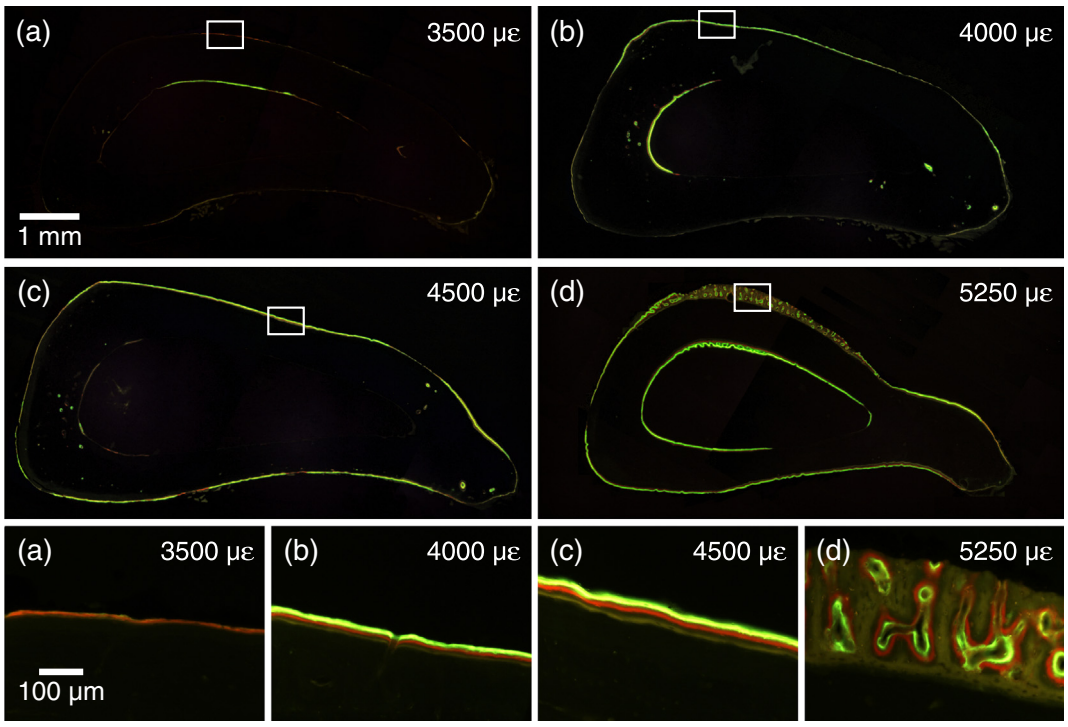

Fig. 5. Representative epifluorescent light micrographs showing labeled periosteal surfaces on transverse sections of whole ulnae subjected to peak compressive strain levels of (a) 3500, (b) 4000, (c) 4500, and (d) 5250 microstrain during *in vivo* ulnar loading. Higher magnification images taken within the inset boxes show individual tetracycline (faint yellow), alizarin (red), and calcein (green) labels (bottom to top) at locations of maximum compressive strain on periosteal surfaces. Contralateral controls and ulnae loaded at 3000 microstrain did not produce measurable levels of periosteal bone formation as evidenced by minimal labeled surface and undetectable interlabel separation (not shown). Ulnae loaded at 3500 microstrain exhibited a detectable but very weak response with minimal labeled surface and minimal interlabel separation. Ulnae loaded at 4000 and 4500 microstrain produced new lamellar bone with 4500 microstrain providing the most robust response shown by interlabel spacing. Ulnae load at 5250 microstrain exhibited significant woven bone formation.

the alizarin-calcein label pair was not affected by increased strain levels, and differences between loaded ulnae and contralateral controls were not statistically significant ($p > 0.28$, ANOVA). The pooled mean (±standard deviation) endosteal MS/BS in loaded ulnae and contralateral controls was 15.1 (15.6) and 22.2 (22.1) percent, respectively, for the alizarin-calcein label pair.

Discussion

In vivo ulnar loading in rabbits provided a dose-dependent anabolic stimulus for periosteal bone formation at peak ulnar compressive strains ranging 3500–4500 microstrain, with 4500 microstrain producing the most robust lamellar bone formation. Contralateral controls and strain levels at 3000 microstrain did not produce measurable bone formation, while strain levels at 5250 microstrain produced significant woven bone on periosteal surfaces. In contrast, rats and mice exhibit periosteal bone formation at strain levels <2000 microstrain for lamellar bone [9,10,16,17,37] and <3000 microstrain for woven bone [13,16,37]. Thus, rabbits required greater strain magnitudes to produce lamellar and woven bone on periosteal surfaces of ulnae compared with rats and mice.

The reason for species-specific differences in strain thresholds for periosteal bone formation in rabbits compared with rodents is not immediately clear and warrants further investigation. One potential explanation is differences in basal periosteal bone formation levels and mechanosensitivity between rabbits and rodents. In this study, the pooled mean (±standard deviation) basal levels of MS/BS and MAR for the ulnae of skeletally-mature rabbits were 9 (10) % (Fig. 6) and 1.2 (0.1) μm/day, respectively, which is comparable to measurements at other cortical bone sites in rabbits [25,29]. Ulnar loading increased MS/BS and MAR to a maximum mean value of ~35% (Fig. 6) and ~1.4 μm/day, respectively, for lamellar bone formation at 4500 microstrain (Fig. 6). In contrast, mean basal levels of MS/BS and MAR in adult (7–8 m/o) rat ulnae were 25–30% and ~0.9 μm/day, respectively, which was increased to ~75% and ~2.5 μm/day, respectively, at ~4000 microstrain using an identical ulnar loading protocol [10]. Skeletal growth in rats continues well past sexual maturity [38] such that already active modeling may be more readily stimulated by exogenous loading.

Rabbits normally exhibit active Haversian remodeling within the intracortical envelope [22–27] while rats and mice do not [1,20–23], which may also factor into a species-dependent predisposition for periosteal bone formation in rodents. Thus, rabbits exhibited remodeling within the intracortical envelope in addition to the periosteal and endocortical envelopes (Fig. 5), in contrast to rodents which normally exhibit remodeling in only the periosteal and endocortical envelopes. Nonetheless, rodent models will remain advantageous in the use of powerful transgenic models, including knockouts and knockins, for studying molecular mechanisms in bone mechanobiology [42]. There are currently no comparable transgenic rabbit models utilized in skeletal research; however, transgenic rabbits have been developed to study other human diseases, primarily cardiovascular disease [43,44], and were reported to exhibit different skeletal phenotypes [45].

The rabbit ulnar loading model was developed by adapting methods from established rat ulnar loading models with two primary modifications in implementation. Rabbit ulnae required instrumentation capable of greater applied axial loads to reach anabolic levels of strain (Fig. 4b) due to rabbit ulnae exhibiting a ~3-fold greater size (length and cortical diameter) compared with rat ulnae. Rabbits also required injected anesthesia, rather than inhaled anesthesia, to achieve proper sedation during ulnar loading and recovery assisted by an antagonist to the anesthetic. These differences in implementation had no affect on the model repeatability. Variability in measurements of MS/BS and MAR in rabbits was comparable to that exhibited by rodent ulnar loading models [9,10,16,17,37]. Moreover, the periosteal strain distribution within loaded

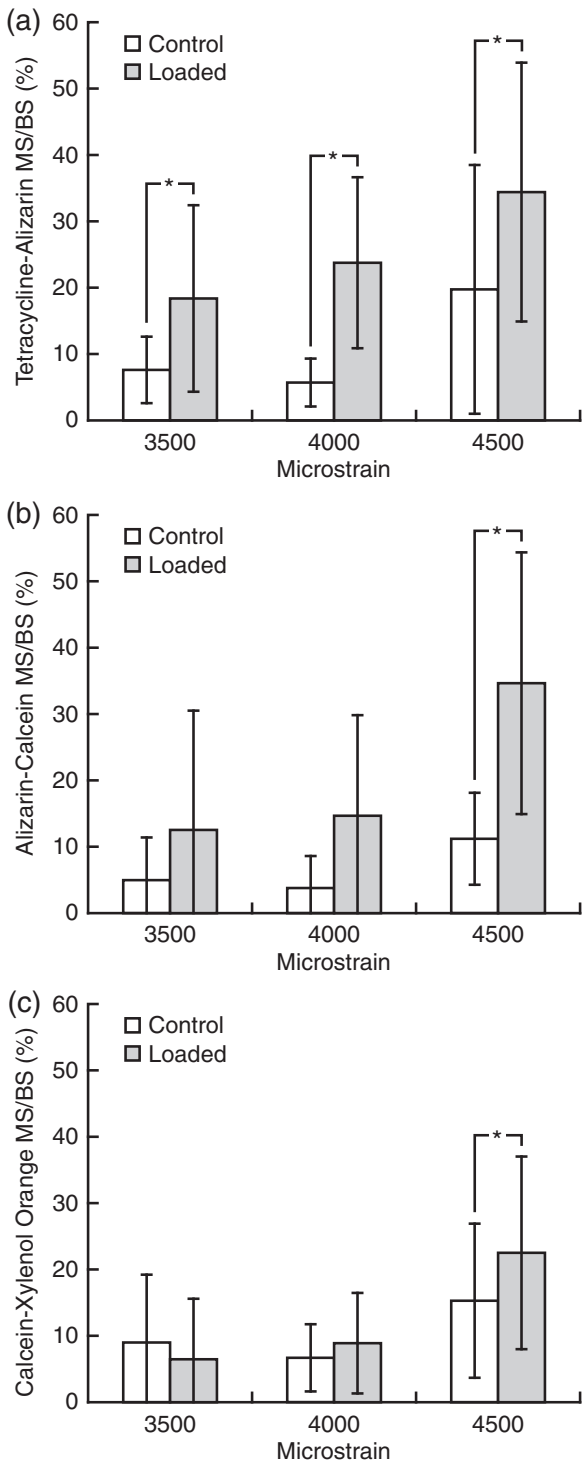

Fig. 6. Periosteal mineralizing surface (MS/BS) measured in ulnae subjected to peak compressive strain levels of 3500, 4000, and 4500 microstrain during *in vivo* ulnar loading, compared with contralateral controls, for each pair of consecutive labels (Fig. 2): (a) tetracycline-alizarin (days 7–14), (b) alizarin-calcein (days 14–21), and (c) calcein-xylenol orange (days 21–28). Error bars show one standard deviation of the mean. MS/BS was elevated in loaded ulnae compared with contralateral controls for each interlabel pair at 4500 microstrain and for tetracycline-alizarin at all strain levels ($^*p < 0.05$ loaded > control, paired *t*-test). MS/BS exhibited an overall increase with increased strain levels for each interlabel pair ($p < 0.05$, ANOVA). All measured data for dynamic histomorphometry are available in the Appendix as Supplementary Content.

ulnae (Fig. 3) and load-strain calibrations (Fig. 4) were comparable to measurements in rats [14,15] considering scaling due to differences in load/strain magnitudes and ulna size.

The results of this study suggest that bone adaptation during rabbit ulnar loading is tightly controlled and can provide an alternative model which may be more translatable for human cortical bone mechanobiology than rodent models. Basal periosteal MS/BS and MAR have been measured to be ≤10% and ≤1 μm/day, respectively, at multiple cortical bone sites within nonhuman primates [39–41], as well as in human iliac crest biopsies [46], similar to measurements in this study. Rabbits are also well-suited for preclinical investigations of osteopenia and pharmaceutical interventions as rabbits experience cortical bone loss after ovariectomy [29], and respond to PTH [25,26], bisphosphonates [28,29], and cathepsin K inhibitors [29]. Thus, rabbit models could provide an alternative for preclinical pharmaceutical investigations that otherwise require more costly and challenging nonhuman primate models [29]. Moreover, rabbit ulnar loading could be used to investigate the effects of aging and pharmaceutical interventions on the mechanical regulation of cortical bone adaptation.

Acknowledgments

This research was supported by a grant from the Investigator Initiated Studies Program of Merck Sharp & Dohme Corp. The authors thank the staff of the Freimann Life Science Center at Notre Dame for their assistance in caring for the rabbits.

Appendix A. Supplementary data

Supplementary data to this article can be found online at http://dx.doi.org/10.1016/j.bone.2015.01.022.

References

[1] Robling AG, Burr DB, Turner CH. Skeletal loading in animals. J Musculoskelet Neuronal Interact 2001;1:249–62.
[2] Liskova M, Hert J. Reaction of bone to mechanical stimuli. Part 2. Periosteal and endosteal reaction of tibial diaphysis in rabbit to intermittent loading. Folia Morphol (Praha) 1971;19:301–17.
[3] Lanyon LE, Rubin CT. Static vs. dynamic loads as an influence on bone remodeling. J Biomech 1984;17:897–905.
[4] Rubin CT, Lanyon LE. Regulation of bone formation by applied dynamic loads. J Bone Joint Surg 1984;66A:397–402.
[5] Turner CH, Ahkter MP, Raab DM, Kimmel DB, Recker RR. A non-invasive, in vivo model for studying strain adaptive bone modeling. Bone 1991;12:73–9.
[6] Gross TD, Srinivasan S, Liu CC, Clemens TL, Bain SD. Noninvasive loading of the murine tibia: an in vivo model for the study of mechanotransduction. J Bone Miner Res 2002;17:493–501.
[7] Burr DB, Milgrom C, Boyd RD, Higgins WL, Robin G, Radin EL. Experimental stress fractures of the tibia: biological and mechanical aetiology in rabbits. J Bone Joint Surg 1990;72B:370–5.
[8] Torrance AG, Mosely JR, Suswillo RFL, Lanyon LE. Noninvasive loading of the rat ulna in vivo induces a strain-related modeling response uncomplicated by trauma or periosteal pressure. Calcif Tissue Int 1994;54:241–7.
[9] Hsieh Y-F, Turner CH. Effects of loading frequency on mechanically induced bone formation. J Bone Miner Res 2001;16:918–24.
[10] Hsieh Y-F, Robling AR, Ambrosius WT, Burr DB, Turner CH. Mechanical loading of diaphyseal bone in vivo: the strain threshold for an osteogenic response varies with location. J Bone Miner Res 2001;16:2291–7.
[11] Robling AG, Duijvelaar KM, Geevers JV, Ohashi N, Turner CH. Modulation of appositional and longitudinal bone growth in the rat ulna by applied static and dynamic force. Bone 2001;29:105–13.
[12] Robling AR, Hinant FM, Burr DB, Turner CH. Improved bone structure and strength after long-term mechanical loading is greatest if loading is separated into short bouts. J Bone Miner Res 2002;17:1545–54.
[13] Hsieh Y-F, Silva MJ. In vivo fatigue loading of the rat ulna induces both formation and resorption and leads to time-related changes in bone mechanical properties and density. J Orthop Res 2002;20:764–71.
[14] Kotha SP, Hsieh Y-F, Strigel RM, Müller R, Silva MJ. Experimental and finite element analysis of the rat ulnar loading model–correlations between strain and bone formation following fatigue loading. J Biomech 2004;37:541–8.
[15] Uthgenannt BA, Silva MJ. Use of the rat forelimb compression model to create discrete levels of bone damage in vivo. J Biomech 2007;40:317–24.
[16] Lee KCL, Maxwell A, Lanyon LE. Validation of a technique for studying functional adaptation of the mouse ulna in response to mechanical loading. Bone 2002;31:407–12.
[17] De Souza RL, Matsuura M, Eckstein F, Rawlinson S, Lanyon LE, Pitsillides AA. Non-invasive axial loading of mouse tibiae increases cortical bone formation and modifies trabecular organization: a new model to study cortical and cancellous compartments in a single loaded element. Bone 2005;37:810–8.

[18] Fritton JC, Myers ER, Wright TM, van der Meulen M. Loading induces site-specific increases in mineral content assessed by micro-computed tomography of the mouse tibia. Bone 2005;36:1030–8.
[19] Main RP, Lynch ME, van der Meulen M. In vivo tibial stiffness is maintained by whole bone morphology and cross-sectional geometry in growing female mice. J Biomech 2010;43:2689–94.
[20] Hagino H, Raab DM, Kimmel DB, Akhter MP, Recker RR. Effect of ovariectomy on bone response to in vivo external loading. J Bone Miner Res 1993;8:347–57.
[21] Sietsema WK. Animal models of cortical porosity. Bone 1995;17:297S–305S.
[22] Bellino FL. Nonprimate animal models of menopause: workshop report. Menopause 2000;7:14–24.
[23] Turner AS. Animal models of osteoporosis—necessity and limitations. Eur Cell Mater 2001;1:66–81.
[24] Nakamura T, Hirai T, Suzuki K, Orimo H. Osteonal remodeling and mechanical properties of the femoral cortex in rabbits treated with 24R,25$(OH)_2D_3$. Calcif Tissue Int 1992;50:74–9.
[25] Hirano T, Burr DB, Turner CH, Sato M, Cain RL, Hock JM. Anabolic effects of human biosynthetic parathyroid hormone fragment (1–34), LY333334, on remodeling and mechanical properties of cortical bone in rabbits. J Bone Miner Res 1999;14:536–45.
[26] Mashiba T, Burr DB, Turner CH, Sato M, Cain RL, Hock JM. Effects of human parathyroid hormone (1-34), LY333334, on bone mass, remodeling, and mechanical properties of cortical bone during the first remodeling cycle in rabbits. Bone 2001; 2001:538–47.
[27] Hedgecock NL, Hadi T, Chen AA, Curtiss SB, Martin RB, Hazelwood SJ. Quantitative regional associations between remodeling, modeling, and osteocyte apoptosis and density in rabbit tibial midshafts. Bone 2007;40:627–37.
[28] Allen MR, Turek JJ, Phipps RJ, Burr DB. Greater magnitude of turnover suppression occurs earlier after treatment initiation with risedronate than alendronate. Bone 2011;49:128–32.
[29] Pennypacker BL, Duong LT, Cusick TE, Masarachia PJ, Gentile MA, Gauthier J-Y, et al. Cathepsin K inhibitors prevent bone loss in estrogen-deficient rabbits. J Bone Miner Res 2011;26:252–62.
[30] Masoud I, Shapiro F, Kent R, Moses A. A longitudinal study of the growth of the New Zealand white rabbit: cumulative and biweekly incremental growth rates for body length, body weight, femoral length, and tibial length. J Orthop Res 1986;4:221–31.
[31] Deuerling JM, Rudy DJ, Niebur GL, Roeder RK. Improved accuracy of cortical bone mineralization measured by polychromatic microcomputed tomography using a novel high mineral density composite calibration phantom. Med Phys 2010;37: 5138–45.
[32] Yang H, Butz KD, Duffy D, Niebur GL, Nauman EA, Main RP. Characterization of cancellous and cortical bone strain in the in vivo mouse tibial loading model using microCT-based finite element analysis. Bone 2014;66:131–9.
[33] Bonfield W, Clark EA. Elastic deformation of compact bone. J Mater Sci 1973;8: 1590–4.
[34] Lipman NS, Phillips PA, Newcomer CE. Reversal of ketamine/xylazine anesthesia in the rabbit with yohimbine. Lab Anim Sci 1987;37:474–7.
[35] Diehl K-H, Hull R, Morton D, Pfister R, Rabemampianina Y, Smith D, et al. A good practice guide to the administration of substances and removal of blood, including routes and volumes. J Appl Toxicol 2001;21:15–23.
[36] Parfitt AM, Drezner MK, Glorieux FH, Kanis JA, Malluche H, Meunier PJ, et al. Bone histomorphometry: standardization of nomenclature, symbols, and units. J Bone Miner Res 1987;2:595–610.
[37] Chen JC, Beaupré GS, Carter DR. An approach to quantifying bone overloading and hypertrophy with applications to multiple experimental studies. Bone 2010;46: 322–9.
[38] Kilborn SH, Trudel G, Uhthoff H. Review of growth plate closure compared with age at sexual maturity and lifespan in laboratory animals. Contemp Top Lab Anim Sci 2002;41:21–6.
[39] Fox J, Miller MA, Newman MK, Recker RR, Turner CH, Smith SY. Effects of daily treatment with parathyroid hormone 1–84 for 16 months on density, architecture and biomechanical properties of cortical bone in adult ovariectomized rhesus monkeys. Bone 2007;41:321–30.
[40] Kostenuik PJ, Smith SY, Jolette J, Schroeder J, Pyrah I, Ominsky MS. Decreased bone remodeling and porosity are associated with improved bone strength in ovariectomized cynomolgus monkeys treated with denosumab, a fully human RANKL antibody. Bone 2011;49:151–61.
[41] Pennypacker BL, Chen CM, Zheng H, Shih M-S, Belfast M, Samadfam R, et al. Inhibition of cathepsin K increases modeling-based bone formation, and improves cortical dimension and strength in adult ovariectomized monkeys. J Bone Miner Res 2014; 29:1847–58.
[42] Niziolek PJ, Farmer TL, Cui Y, Turner CH, Warman ML, Robling AG. High-bone-mass-producing mutations in the Wnt signaling pathway result in distinct skeletal phenotypes. Bone 2011;49:1010–9.
[43] Fan J, Challah M, Watanabe T. Transgenic rabbit models for biomedical research: current status, basic methods and future perspectives. Pathol Int 1999;49:583–94.
[44] Bosze Z, Hiripi L, Carnwath JW, Niemann H. The transgenic rabbit as model for human diseases and as a source of biologically active recombinant proteins. Transgenic Res 2003;12:541–53.
[45] Martiniakova M, Omelka R, Chrenek P, Ryban L', Parkanyi V, Grosskopf B, et al. Changes of femoral bone tissue microstructure in transgenic rabbits. Folia Biol (Praha) 2005;51:140–4.
[46] Ma YL, Zeng QQ, Chian AY, Burr D, Li J, Dobnig H, et al. Effects of teriparatide on cortical histomorphometric variables in postmenopausal women with or without prior alendronate treatment. Bone 2014;59:139–47.